Fibers and Polymers 2021, Vol.22, No.8, 2119-2126
DOI 10.1007/s12221-021-0920-2

ISSN 1229-9197 (print version)
ISSN 1875-0052 (electronic version)

Polypyrrole/Organic Sulfonic Acid Coated Activated Carbon Fiber Felt as Flexible Supercapacitor with High-performance

Huiyu Yang[1,2], Jie Xu[2], Lisha Zhai[2], Xin Liu[2], Bo Deng[2]*, and Weilin Xu[2]*

[1]*College of Material Science and Engineering, Wuhan Institute of Technology, Wuhan 430073, China*
[2]*State Key Laboratory of New Textile Materials and Advanced Processing Technologies, Wuhan Textile University, Wuhan 430200, China*

(Received August 5, 2020; Revised October 12, 2020; Accepted November 1, 2020)

Abstract: Polypyrrole (PPy) was deposited onto carbon fiber felt (CFF) by in-situ polymerization to prepare CFF/PPy composite textile as free-standing and flexible electrode for supercapacitor. Electrochemical performance was characterized by cyclic voltammetry (CV), electrochemical impedance (EIS) and constant current charge-discharge technology. The results show that the doping of organic sulfonic acid further improved the electrochemical performance of electrode materials. Areal capacitance, energy density and power density of the CFF/PPy/TsOH are as high as 5943 $mF \cdot cm^{-2}$, 1739 $\mu Wh \cdot cm^{-2}$, 1450 $\mu W \cdot cm^{-2}$, respectively (at a current density of 0.8 $mA \cdot cm^{-2}$). Overall, this flexible textile electrode is promising to be used as wearable electronic device.

Keywords: Carbon fiber felt, Polypyrrole, Fabric electrode, Supercapacitor, Organic sulfonic acid

Introduction

With the growing demand for portable and wearable electronic devices, flexible supercapacitor has received widespread attention as a novel energy storage device due to its excellent flexibility/deformability, high power density, long cycling stability and fast charge/discharge rate [1-3]. Ideal advanced wearable electronic device should have the characteristics of light weight, breathability, and flexibility. Traditional flexible substrates such as fabrics and cloths are difficult to be replaced by other substrates due to their inherent flexibility and breathability. Areal capacitance, energy, and power densities are three key performances for flexible supercapacitor due to limited space and surface area [4,5]. Except for the continuous pursuit of high electrochemical performance, cost-effectiveness and environmental friendliness have also been a widespread concern for flexible super-capacitor. To satisfy these requirements, suitable flexible electrodes were prepared by depositing active materials on various low-cost substrates, such as plastic [6], cotton fabric [7], and cellulose paper [8]. However, the design and preparation of flexible electrode materials with high electrochemical performance and good flexibility through a simple fabrication process has become an important challenge for the preparation of supercapacitor [9].

According to the charge storage mechanism, capacitors could be divided into the electrical double-layer capacitor (EDLC) and the pseudo-capacitor [2]. EDLCs often uses carbon materials as electrodes to store the energy derived from the charge separations occurred at the electrode/ electrolyte interface. While the main electrochemically active material used for pseudo-capacitors are transition metal oxides/sulfides or conductive polymers (such as PPy, polyaniline, polythiophene, etc.). Generally, pseudo-capacitor has a relatively larger capacitance than EDLC, which may be due to the fact that energy is stored through a reversible redox reaction [10].

Among these electrochemically active materials, conductive polymers have been widely used for flexible supercapacitors owing to their high electrical conductivity, high inherent flexibility and diversified preparation methods [11-13]. PPy, identified with the continuous conductive framework, fast transport of charges and ions, was intensively used as electrochemically active material for flexible supercapacitor. However, untreated PPy is not suitable for processing due to its insolubility and non-melting properties. To improve the conducting performance of PPy and endow it with various morphologies, many metal oxides [14,15], carbon materials (such as carbon nanotubes [16,17], graphene oxide [18], etc.), and various sulfonates or organic sulfonic acids [19,20] have been widely used in in-situ doping polymerization of Py.

Especially, the doping of organic sulfonic acid not only facilitates polymerization of Py but also acts as a surfactant and proton agent which effectively improving the chemical stability, mechanical stability, and proton conductivity of the Ppy [21,22].

Furthermore, base material of electrode is also crucial for supercapacitor. The base material should have affluent electrolyte ion-diffusion channels, excellent electrical conductivity, and excellent flexibility to adapt to various conditions at low cost [9]. Carbon fiber felt (CFF) [23], as a carbon-based material, has a unique porous structure and flexibility. It can be directly used as an integrated electrode without binders and conductive additives. Moreover, the free-standing CFF electrode not only supports the adhered conductive polymer but also exhibits ion adsorption activity.

*Corresponding author: dengjianguo88@outlook.com
*Corresponding author: weilin_xu@hotmail.com

Herein, we chose CFF as the base material of electrode. PPy was in-situ polymerized onto CFF with the dopants, p-toluene sulfonic acid (TsOH) or β-naphthalene sulfonic acid (2-NSA), respectively, to prepare flexible textile electrodes with high-performance. CFF base material showed both excellent electrolyte permeability with promoted ion/electron transfer and hierarchical pore structure with enhanced capacitance. The effect of added dopants on the conductivity of PPy was further investigated. It was found that added dopants significantly improved the rate capability, areal capacitance, and energy density of CFF/PPy electrode material. A highest energy density of 5943 $mF \cdot cm^{-2}$ at a current density of 0.8 $mA \cdot cm^{-2}$ could be achieved for CFF/PPy/TsOH. Besides, the CFF/PPy/TsOH electrode material showed good flexibility under different bending degrees without altering the current. Overall, this work provides a new approach for the fabrication of flexible high energy density devices.

Experimental

Carbon fiber felt (CFF), with a thickness of 3.0 mm, was supplied by Wuhan Textile University. Pyrrole (Py) was obtained from Aladdin Reagent Co., Ltd. Cetyltrimethylammonium bromide (CTAB, 99 %), sodium dodecyl benzene sulfonate (SDBS, 99.9 %), TsOH (≥ 98 %), and 2-NSA (≥ 98 %) were purchased from Sinopharm Chemical Reagent Co., Ltd. Ferric chloride hexahydrate ($FeCl_3 \cdot 6H_2O$, ≥ 99.0 %) and sodium chloride (NaCl, ≥ 99.8 %) were supplied by Shanghai Chemical Company. The deionized water with a resistivity of 10-16 MΩ·cm was obtained from a Milli-Q Plus 185 water purification system (Millipore, Bedford, USA) in the whole experimental process. All the above chemicals were used without any further purification.

Preparation of PPy-coated CFF

PPy was coated onto the CFF *via* in-situ polymerization of Py as illustrated in Figure 1. The specific preparation process of CFF/PPy/TsOH is as follows: initially, the commercial CFF with an area of 3.0 cm^2 (1 cm×3 cm) was cleaned by ultrasonic to remove surface impurities and then dried at 60 °C for 4 hours. The cleaned CFF was placed in 100 m*l* Py mixture containing pyrrole (0.1 M), CTAB (0.002 M), SDBS (0.002 M), and TsOH (0.1 M) and magnetically stirred for 30 minutes. Subsequently, 100 m*l* of $FeCl_3$ aqueous solution (0.5 M) was added dropwise to the Py mixture with a temperature of 5 °C under magnetic stirring. Then polymerization was carried out for 2 further hours under stirring. Finally, CFF was brought out and washed in turn with deionized water and ethanol to remove excess reagents and vacuum-dried under 60 °C to constant weight. The obtained composited CFF sample was denoted as CFF/PPy/TsOH.

The preparation process of CFF/PPy/2-NSA was as follows: cleaned CFF with the size of 1×3 cm was placed in 100 m*l* Py mixture containing pyrrole (0.1 M), CTAB (0.002 M), and SDBS (0.002 M) in and stirred for 30 minutes. Subsequently, 100 m*l* $FeCl_3$ aqueous solution (0.5 M) was added dropwise to the Py mixture with a temperature of 5 °C under stirring. Then polymerization was carried out for 2 further hours under stirring. After the reaction was completed, the resulting CFF was immersed in 1 M aqueous solution of 2-NSA for 30 minutes. Finally, CFF was brought out and washed in turn by deionized water and ethanol to remove excess reagents and vacuum-dried to constant weight under 60 °C. The obtained sample was

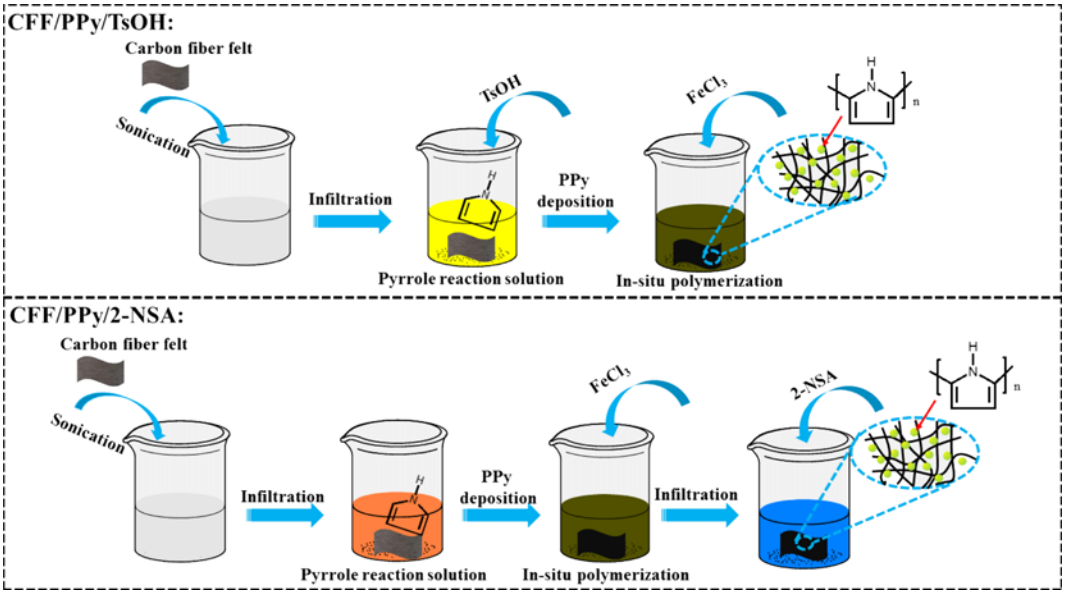

Figure 1. Schematic illustration of the fabrication of CFF/PPy/TsOH and CFF/PPy/2-NSA.

denoted as CFF/PPy/2-NSA. For comparison, the samples without TsOH or 2-NSA treatment was denoted as CFF/PPy.

Characterization

Surface morphologies of CFF were investigated by a scanning electron microscopy (SEM, JSM-6510LV, JEOL, Japan). The electrical conductivity of the samples was obtained at room temperature by an RTS-9 four-point probe resistivity meter (RTS-9, 4Probes Tech., China) with copper electrode. The electrochemical performances of fabric electrodes (CFF/PPy, CFF/PPy/TsOH, and CFF/PPy/2-NSA), except for CV test, was evaluated by Autolab PGSTAT302N potentiostat/constant current analyzer (Autolab PGSTAT302N, Metrohm AG, Switzerland) in a two-electrode system. The CV measurements were carried out in a three-electrode system with the potential ranged from 0 to 0.8 V and the scan rates varied from 5 to 50 $mV \cdot s^{-1}$. The CFF substrate was used as the working electrode; a platinum plate and a KCl saturated calomel electrode (SCE, CH Instrument, China) were used as counter and reference electrodes, respectively. The EIS plots were recorded from 10 mHz to 100 kHz with an impedance amplitude of 5 mV at open circuit potential. The constant current charge-discharge (GCD) cycling experiments were analyzed over a range of 0-0.8 V by a multichannel CT2001A battery tester (CT2001A, Wuhan Land Electronics, China) at various current densities. All above electrochemical measurements were carried out in 1.0 M aqueous solution of NaCl. The mechanical properties of the CFF were evaluated by using a YG 028 universal materials testing machine (Wenzhou Fangyuan Instrument, Co. Ltd., Zhejiang, China) at a strain rate of 10 mm/min. The sample size is 1 cm×3 cm, and each sample was measured 5 times to obtain the average value.

Results and Discussion

The surface morphologies of untreated and treated CFF were investigated by SEM as shown in Figure 2. The untreated CFF (Figure 2a) was fabricated by entanglement and overlap of carbon fibers. Bundle of fibers with a diameter of about 16 μm formed a three-dimensional interconnected and porous network structure. The rich porous network structure endows CFF with higher specific surface area and other outstanding properties of the foam such as bendability.

After in situ polymerization (Figure 2b), PPy particles with different sizes adhered to the surface of the CFF fiber and the inside pores of the CFF fabric. Compared with CFF/PPy, more densely packed small particles on the fiber surface could be found in 2-NSA (Figure 2c) or TsOH

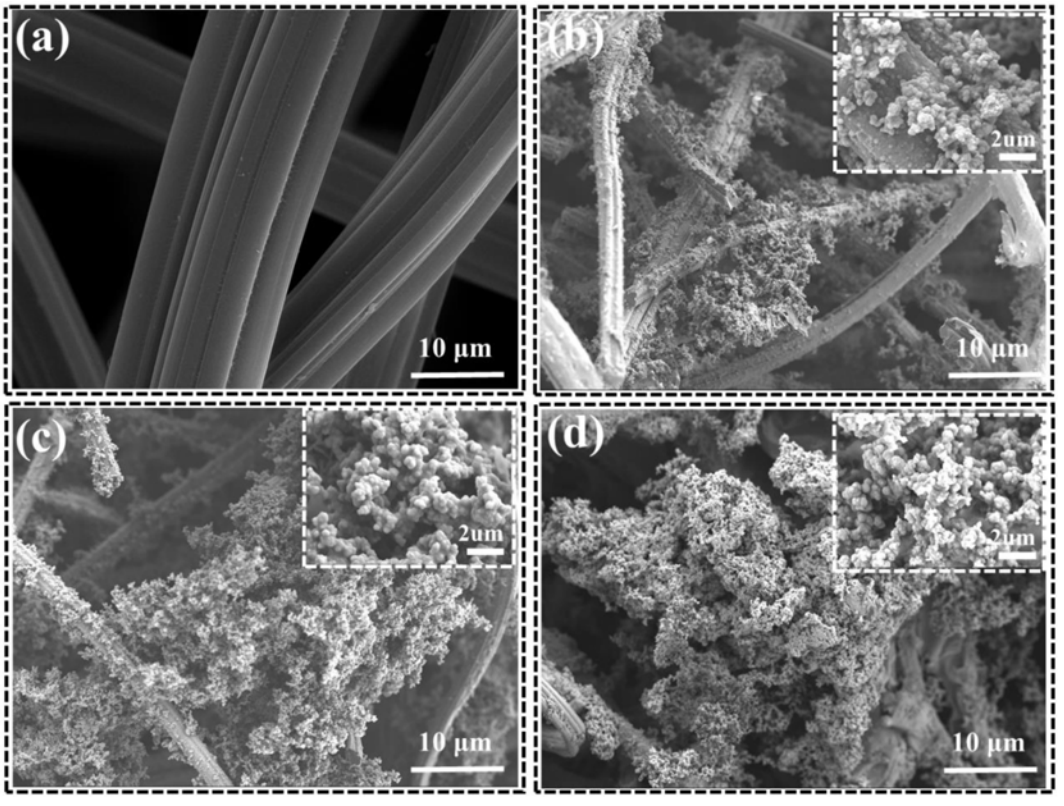

Figure 2. SEM images of (a) untreated CFF, (b) CFF/PPy, (c) CFF/PPy/2-NSA, and (d) CFF/PPy/TsOH (inset is the image at high magnification).

treated (Figure 2d) CFF. This is mainly because of the enhancement effect of TsOH or 2NSA to the polymerization degree and the cross-linking of PPy. Thereby the bulk density of fiber surface active materials was increased after TsOH or 2-NSA treatment [24]. However, the anion volume of 2-NSA is larger than that of TsOH, and the corresponding larger steric hindrance effectively reduced the crosslinking reaction between PPy chains [25,26]. Therefore, the bulk density of CFF/PPy/2-NSA was lower than that of CFF/PPy/TsOH.

The electrochemical performances of the CFF/PPy, CFF/PPy/2-NSA and CFF/PPy/TsOH were compared by adopting their textile samples as electrode in a two-electrode system using 1.0 M NaCl as electrolyte. The CV curves of CFF/PPy, CFF/PPy/2-NSA, and CFF/PPy/TsOH at a scan rate of 5 $mV \cdot s^{-1}$ with the potential window ranging from 0 to 0.8 V are shown in Figure 3a. The curves of all samples exhibit a large enclosed area with approximately rectangular shapes without obvious redox peaks, indicating that the electrodes were charged and discharged at a pseudo-constant rate during the entire CV process [27]. In general, the specific capacitance of the electrode material is proportional to the enclosed area of the CV curve. As shown in Figure 3a, CFF/PPy/TsOH and CFF/PPy/2-NSA composite electrodes showed a larger enclosed area than CFF/PPy, demonstrating a higher specific capacitance.

EIS was measured to analyze the electronic/ionic conductivity of the electrode materials during the charge-discharge progress. The Nyquist plots of CFF/PPy, CFF/PPy/TsOH, and CFF/PPy/2-NSA fabric electrodes in the frequency range of 0.01 Hz to 100 kHz were shown in Figure 3b. The electron transport limited process corresponds to the higher frequency region, which is mainly caused by the internal resistance of the electrode and the resistance of the solution. The restricted diffusion process in the electrolyte corresponds to the low frequency region, indicating that the device has ideal capacitive performance. It can be seen in Figure 3b that all impedance curves composed of a small concave semicircle in the high frequency region and a linear part in the low frequency region. The high-frequency intercept of the semicircle on the real axis is mainly related to the equivalent series resistance composed of the electrode and the electrolyte. The charge transfer resistance is represented by the diameter of the semicircle. The impedance curves were fitted with an equivalent circuit according to the inset of Figure 3b. The equivalent circuit is mainly composed of

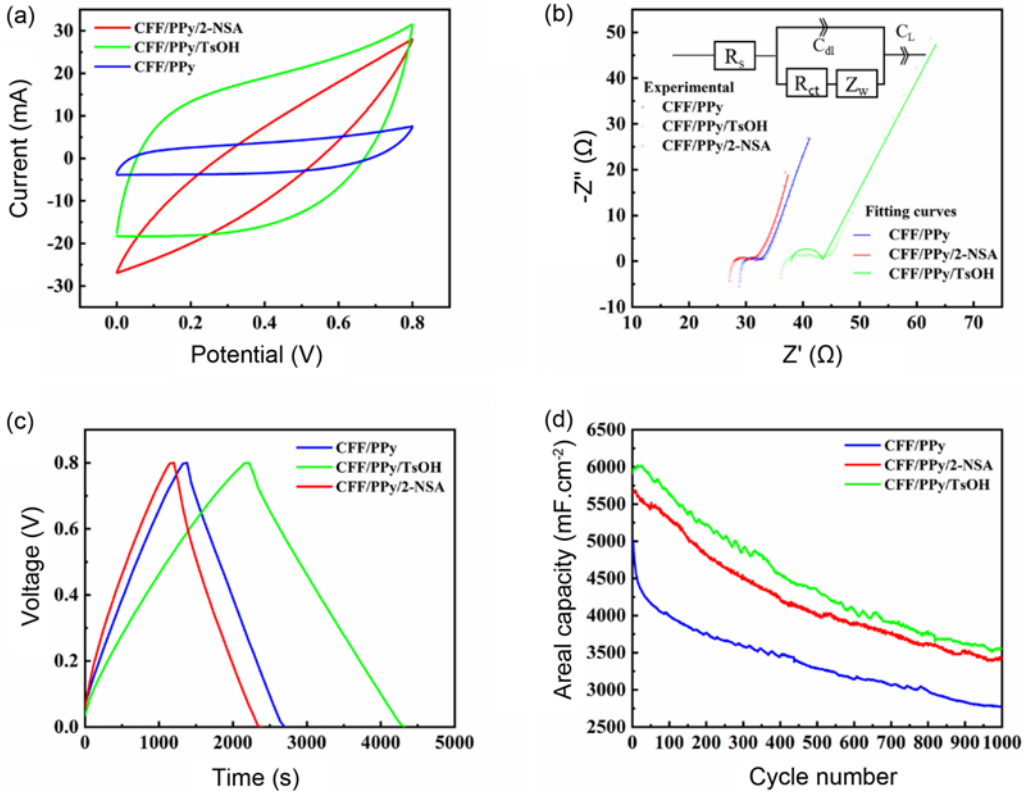

Figure 3. (a) CV curves of the CFF/PPy, CFF/PPy/2-NSA, and CFF/PPy/TsOH electrodes based supercapacitors at a scan rate of 5 $mV \cdot s^{-1}$, (b) Nyquist plots of CFF/PPy, CFF/PPy/2-NSA and CFF/PPy/TsOH, (c) GCD profiles of CFF/PPy, CFF/PPy/2-NSA, and CFF/PPy/TsOH electrodes at a current density of 0.8 $mA \cdot cm^{-2}$, and (d) cycling stability of CFF/PPy, CFF/PPy/2-NSA, and CFF/PPy/TsOH electrodes at a current density of 0.8 $mA \cdot cm^{-2}$.

Table 1. Fitted EIS parameters of symmetric supercapacitors with various PPy-based electrodes

Electrode	R_s (Ω)	R_{ct} (Ω)
CFF/PPy	31.3	3.2
CFF/PPy/2-NSA	28.2	2.6
CFF/PPy/TsOH	37.9	4.5

electrode and electrolyte resistance (R_s), resistance produced by interface charge transfer (R_{ct}), and Warburg diffusion resistance (Z_w). C_{dl} and C_L are the electric double layer capacitance and limit capacitance of the electrode/electrolyte interface, respectively. The main resistance parameters of supercapacitors are listed in Table 1. The series resistance and the charge transfer resistance increase in a order of CFF/PPy/2-NSA < CFF/PPy < CFF/PPy/TsOH. The relatively low effective resistance of CFF/PPy/2-NSA indicates its high protonation level and high charge transfer efficiency, and therefore can reduce energy loss of CFF/PPy/TsOH capacitor during charging and discharging.

Figure 3c shows the GCD curve of CFF/PPy, CFF/PPy/2-NSA and CFF/PPy/TsOH electrodes at a current density of 0.8 $mA \cdot cm^{-2}$. All curves have a nearly symmetrical triangle, indicating that the device has excellent ion and electron transport and capacitance performance [10]. In the GCD test, the IR_{drop} during charging and discharging is usually caused by the overall internal resistance of the device, such as electrolyte resistance, electrode resistance, and contact resistance between the electrolyte/electrode interfaces. Energy storage devices with low internal resistance will reduce energy loss and avoid generating more heat during GCD process [28]. According to the GCD test results, the IR_{drop} value decreases in the order of CFF/PPy > CFF/PPy/2-NSA > CFF/PPy/TsOH, indicates that TsOH can improve capacitor performance and promote electrons or proton transmission rate. The specific capacitance was evaluated using the following equation based on the GCD data.

$$C_m = \frac{I \times t}{V \times S} \tag{1}$$

where *I*, *t*, *S*, and *V* represents the constant charge/discharge current, the discharge time, the area of working electrode material, and the voltage change upon discharging (excluding the IR drop, IR_{drop} is the IR voltage drop), respectively. The specific capacitance is about 5126 and 5943 $mF \cdot cm^{-2}$ for CFF/PPy/2-NSA and CFF/PPy/TsOH at a current density of 0.8 $mA \cdot cm^{-2}$, respectively, which is significantly larger than that of CFF/PPy (4049 $mF \cdot cm^{-2}$). The specific capacitance of CFF/PPy/TsOH is larger than those reported PPy-based fabric electrodes, such as Fe_2O_3/PPy/carbon cloth (382.4 $mF \cdot cm^{-2}$ at a current density of 0.5 $mA \cdot cm^{-2}$ [29], graphene oxide/activated carbon/ PPy (906 $mF \cdot cm^{-2}$) [30]. The higher thickness of the three-dimensional network structure of CFF will load more active materials, which leads to larger area specific capacitance and longer discharge time.

The cycle stability of the supercapacitor was tested by the GCD method at 0.8 $mA \cdot cm^{-2}$ as shown in Figure 3d. The overall capacitance performance of all samples decreased with increased cycle numbers. While the decrease of CFF/PPy was more significantly in the first 150 cycles indicating that its charge-discharge cycle stability is not very good. Generally, the instability of capacitor performance is mainly due to the diffusion of counter-ions in the electrolyte into the backbone of PPy chains or back into the electrolyte during the charge-discharge process, resulting in swell or shrink of the backbone of PPy [31]. The PPy backbone will be destroyed during the repeated swelling or shrinking process, thereby reducing the capacitance performance. The charge-discharge cycle stability of CFF based fabric electrode need to be further improved for its practical applications.

The electrochemical performance of CFF/PPy/TsOH was further analyzed as shown in Figure 4. Figure 4a showed that the GCD curve of CFF/PPy/TsOH exhibited slightly deviated triangle, and there was no obvious IR_{drop} at various current densities from 0.2 to 1.6 $mA \cdot cm^{-2}$, indicating the reversibility of redox reaction in the current range. Figure 4b showed the CV curve of CFF/PPy/TsOH in the scan rate ranging from 5 $mV \cdot s^{-1}$ to 50 $mV \cdot s^{-1}$. With the increased scan rates, the CV curves with a constant quasi-rectangular shape indicating that CFF/PPy/TsOH possessed good reversibility within the scan rate ranging from 5 $mV \cdot s^{-1}$ to 50 $mV \cdot s^{-1}$. The specific capacitance (C_{sp}) can be calculated from the CV curve by the following equation:

$$C_{sp} = \frac{\int IdV}{f \times \Delta V \times S} \tag{2}$$

where *I*, *f*, ΔV, and *S* are the response current, the scan rate of the CV curve, the voltage difference, and the area of the active material, respectively. The calculated C_{sp} values for the CFF/PPy and CFF/PPy/TsOH at different scan rates were shown in Figure 4c. It can be seen that the specific capacitance of CFF/PPy/TsOH was greater than CFF/PPy within the scan rates from 5 $mV \cdot s^{-1}$ to 50 $mV \cdot s^{-1}$, which showed that TsOH can significantly improve the capacitance. Especially the specific capacitance of CFF/PPy/TsOH was about 2700 $mF \cdot cm^{-2}$ higher than that of CFF/PPy at a scan rate of 5 $mV \cdot s^{-1}$. However, with the increased scan rate, the C_{sp} values of both CFF/PPy/TsOH and CFF/PPy decreased. This may be attributed to the ion diffusion effect within the active material and at the electrode/electrolyte interface [32].

Figure 4d showed the relative area capacitance of CFF/PPy and CFF/PPy/TsOH at various current densities calculated according to the GCD curves. When the current density increased from 0.2 $mA \cdot cm^{-2}$ to 1.6 $mA \cdot cm^{-2}$, the capacitances of CFF/PPy and CFF/PPy/TsOH dropped to about 79.9 % and 72.5 %, respectively. Impressively, the areal capacitance of CFF/PPy/TsOH based supercapacitor was as high as 5483 $mF \cdot cm^{-2}$ at the current density of

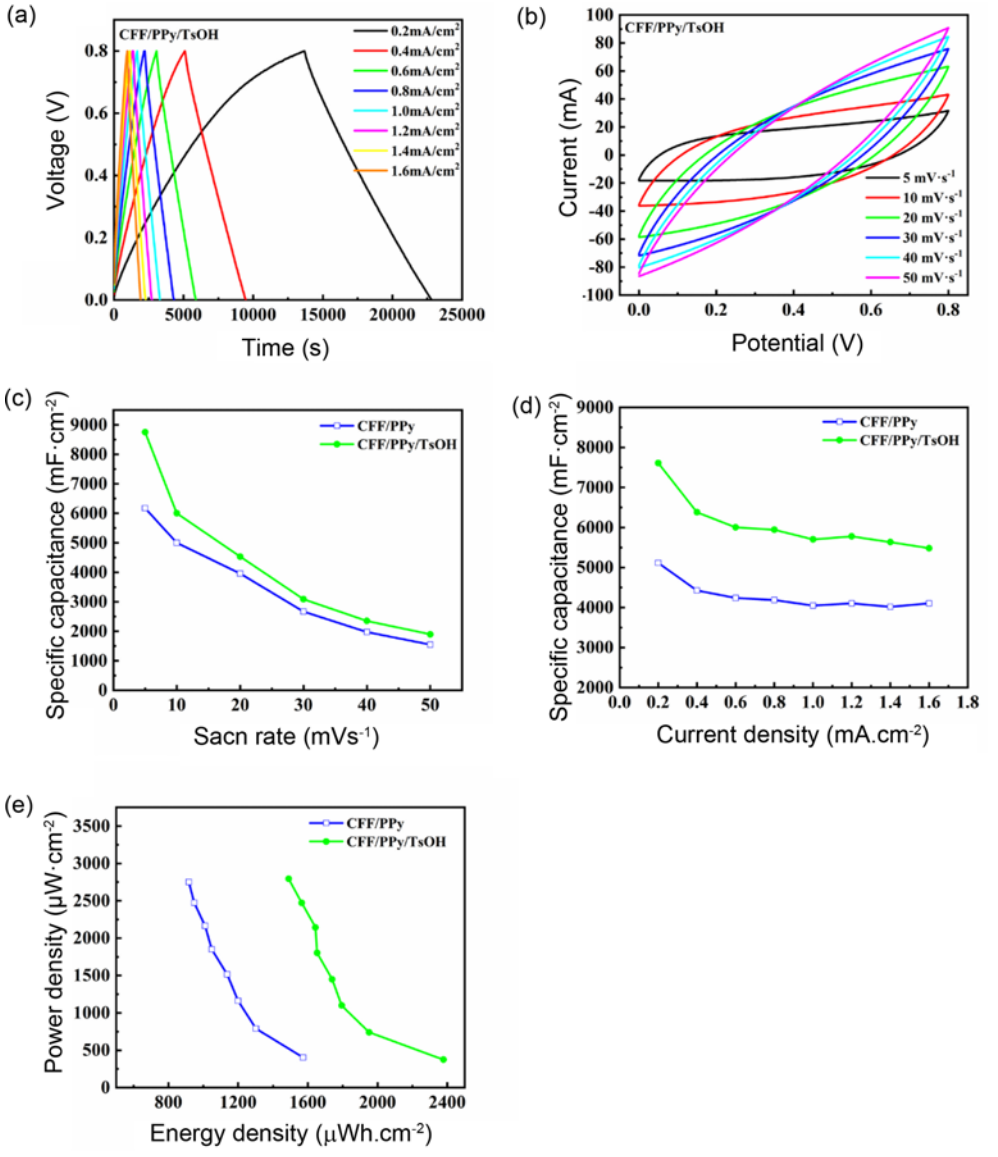

Figure 4. (a) GCD curves of CFF/PPy/TsOH electrode at various current densities, (b) CV curves of CFF/PPy/TsOH electrode at various scan rates, (c) specific capacitance calculated from CV of CFF/PPy and CFF/PPy/TsOH electrodes at different scan rates, (d) specific capacitance of CFF/PPy and CFF/PPy/TsOH electrodes at different current densities, and (e) Ragone plots of CFF/PPy and CFF/PPy/TsOH electrodes.

1.6 mA·cm^{-2}, which is about 1.4 times that of CFF/PPy at the same current density. The excellent rate performance of CFF/PPy/TsOH was attributed to more active materials loaded onto the surface of CFF, which improved the interface charge transfer with the electrolyte. In addition, the stable areal capacitance of CFF/PPy and CFF/PPy/TsOH in the current density range from 0.4 to 1.6 mA·cm^{-2} showed the excellent rate capability of PPy-based supercapacitors.

Figure 4e shows the areal energy density and power density of the as prepared CFF/PPy/TsOH and CFF/PPy. The energy density (E, μWh·cm^{-2}) and power density (P, μW·cm^{-2}) of the supercapacitor were obtained from the following equations [33]:

$$E = \frac{C \times V^2}{2} \tag{3}$$

$$P = \frac{E}{t} \tag{4}$$

where C, V, E, and t are the capacitance of the two-electrode capacitor, the voltage drop during discharge, the energy density, and the discharge time, respectively. CFF/PPy supercapacitor exhibited a high energy density of 1572.4 μWh·cm^{-2} at a power density of 400 μW·cm^{-2}, and

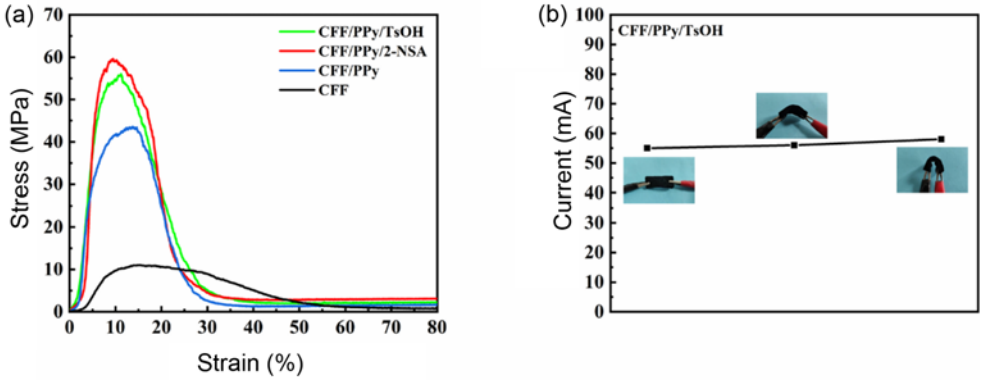

Figure 5. (a) Stress-strain curves of CFF, CFF/PPy, CFF/PPy/2-NSA, and CFF/PPy/TsOH and (b) current of CFF/PPy/TsOH with different curvatures under a constant voltage of 0.8 V.

maintained at 916.7 μWh·cm^{-2} even at a power density of 2700 μW·cm^{-2}. Similarly, CFF/PPy/TsOH supercapacitor also provided excellent energy density from 2378 μWh·cm^{-2} (at a power density of 375 μW·cm^{-2}) to 1489.9 μWh·cm^{-2} (at a power density of 2793 μW·cm^{-2}). The thicker porous three-dimensional structure of CFF provided more space for the residence of active materials. The energy and power density of our supercapacitors were significantly higher than those reported traditional supercapacitors in aqueous electrolytes, such as NC LDH NSs@Ag@CC (78.8 μWh·cm^{-2} at the power density of 785 μW·cm^{-2}) [34], polyaniline/rGO/polyester (54 μWh·cm^{-2} at the power density of 807 μW·cm^{-2}) [35], Li/PANI/FGH/FCC (169.9 μWh·cm^{-2} at the power density of 1000 μW·cm^{-2}) [36], and DN-PGH/PANIPA (155 μWh·cm^{-2} at the power density of 200 μW·cm^{-2}) [37].

The flexibility of fabric electrode was essential for its real application. Figure 5a showed the stress-strain curves of the CFF-based supercapacitors. It can be observed that after being coated by PPy, the breaking strength of the fabric electrode was significantly increased. This may be attributed to the effective interaction between the imine group of PPy and the hydroxyl group of fiber which thereby improved the strength of the substrate [38].

To investigate the electrochemical performance and flexibility of CFF/PPy/TsOH electrode material, the conductivity stability of CFF/PPy/TsOH under different curvatures at a fixed voltage of 0.8 V was shown in Figure 5b. It can be clearly observed that the current was almost unchanged after bent to different degrees, which indicated the stable conductivity of CFF/PPy/TsOH without affected by the bending. This further convinced its suitability in the application as flexible electronics equipment.

Conclusion

In summary, CFF/PPy/TsOH fabric electrode as flexible supercapacitor was successfully fabricated by in-situ polymerization of Py onto three-dimensional porous CFF with the dopant, TsOH. The porous affluent structure of CFF made it load more active materials, thus exhibited excellent conductivity. Moreover, the TsOH dopant effectively increased the polymerization degree of PPy, and endowed the fabric electrode with higher capacitance performance. A specific capacitance up to 5943 mF·cm^{-2} at a current density of 0.8 mA·cm^{-2} in a two-electrode system of CFF/PPy/TsOH was achieved, which was about 1.42 times that of CFF/PPy. Electrochemical measurements proved that added TsOH considerably improved the capacitance of the CFF/PPy electrode. Besides, CFF/PPy/TsOH supercapacitor provided an excellent energy density of 2378 μWh·cm^{-2} at a power density of 375 μW·cm^{-2}. These results confirmed the application potential of CFF/PPy/TsOH fabric electrode as electrodes for flexible supercapacitor.

Acknowledgements

This work was supported by the National Natural Science Foundation of China (Grant 51773158); and the Key Laboratory of Textile Fiber&Product (Wuhan Textile University) (Grant FZXW2017013), Ministry of Education.

References

1. X. Lu, M. Yu, G. Wang, Y. Tong, and Y. Li, *Energy Environ. Sci.*, **7**, 2160 (2014).
2. D. P. Dubal, N. R. Chodankar, D. H. Kim, and P. Gomez-Romero, *Chem. Soc. Rev.*, **47**, 2065 (2018).
3. J. Xu, D. Wang, L. Fan, Y. Yuan, W. Wei, R. Liu, S. Gu, and W. Xu, *Organic Electronics*, **26**, 292 (2015).
4. Y. Ko, M. Kwon, W. K. Bae, B. Lee, S. W. Lee, and J. Cho, *Nat. Commun.*, **8**, 536 (2017).
5. L. Dong, G. Liang, C. Xu, W. Liu, Z. Z. Pan, E. Zhou, F. Kang, and Q. H. Yang, *Nano Energy*, **34**, 242 (2017).
6. Y. Zhong, X. Zhang, Y. He, H. Peng, G. Wang, and G. Xin, *Adv. Funct. Mater.*, **28**, 1801998 (2018).
7. Y. Yang, Q. Huang, L. Niu, D. Wang, C. Yan, Y. She, and

Z. Zheng, *Adv. Mater.,* **29**, 1606679 (2017).
8. L. Dong, C. Xu, Y. Li, Z. Pan, G. Liang, E. Zhou, F. Kang, and Q. H. Yang, *Adv. Mater.,* **28**, 9313 (2016).
9. S. Peng, L. Fan, C. Wei, H. Bao, H. Zhang, W. Xu, and J. Xu, *Cellulose*, **23**, 2639 (2016).
10. S. Peng, L. Fan, C. Wei, X. Liu, H. Zhang, W. Xu, and J. Xu, *Carbohydr. Polym.,* **157**, 344 (2017).
11. M. Gholami, P. M. Nia, and Y. Alias, *Appl. Surf. Sci.,* **357**, 806 (2015).
12. N. A. Kumar, H. J. Choi, Y. R. Shin, D. W. Chang, L. Dai, and J. B. Baek, *Acs Nano.,* **6**, 1715 (2012).
13. J. P. Mensing, A. Wisitsoraat, D. Phokharatkul, T. Lomas, and A. Tuantranont, *Compos. Part B-Eng.*, **77**, 93 (2015).
14. J. Zhu, S. Wei, L. Zhang, Y. Mao, J. Ryu, P. Mavinakuli, A. B. Karki, D. P. Young, and Z. Guo, *J. Phys. Chem. C,* **114**, 16335 (2010).
15. F. N. I. Sari and J.-M. Ting, *Electrochim. Acta,* **320**, 134533 (2019).
16. M. A. A. M. Abdah, N. S. M. Razali, P. T. Lim, S. Kulandaivalu, and Y. Sulaiman, *Mater. Chem. Phys.,* **219**, 120 (2018).
17. H. Zhou, *J. Mater. Sci.: Mater. Electron.,* **29**, 7857 (2018).
18. H. Zhou and H.-J. Zhai, *Org. Electron.,* **37**, 197 (2016).
19. W. Zhou, G. Han, Y. Xiao, Y. Chang, W. Yuan, Y. Li, C. Liu, and Y. Zhang, *Electrochim. Acta,* **176**, 594 (2015).
20. P. Pattananuwat and D. Aht-ong, *Electrochim. Acta,* **224**, 149 (2017).
21. W. Chen, R. Rakhi, and H. N. Alshareef, *J. Mater. Chem. A,* **1**, 3315 (2013).
22. B. Smitha, S. Sridhar, and A. Khan, *J. Membr. Sci.,* **259**, 10 (2005).
23. M. Tian, J. Wu, R. Li, Y. Chen, and D. Long, *Chem. Eng. J.,* **363**, 183 (2019).
24. L. Warren, J. Walker, D. Anderson, C. Rhodes, and L. Buckley, *J. Electrochem. Soc.,* **136**, 2286 (1989).
25. G. Zotti, G. Schiavon, and N. Comisso, *Synth. Met.,* **40**, 309 (1991).
26. J. Lee, D. Kim, and C. Kim, *Synth. Met.,* **74**, 103 (1995).
27. C. Zhang, J. Tian, W. Rao, B. Guo, L. Fan, W. Xu, and J. Xu, *Cellulose,* **26**, 3387 (2019).
28. J. Zhong, L.-Q. Fan, X. Wu, J.-H. Wu, G.-J. Liu, J.-M. Lin, M.-L. Huang, and Y.-L. Wei, *Electrochim. Acta*, **166**, 150 (2015).
29. L. Wang, H. Yang, X. Liu, R. Zeng, M. Li, Y. Huang, and X. Hu, *Angew. Chem., Int. Ed.,* **56**, 1105 (2017).
30. L. Xu, M. Jia, Y. Li, S. Zhang, and X. Jin, *Rsc Adv.,* **7**, 31342 (2017).
31. J. Heinze, B. A. Frontana-Uribe, and S. Ludwigs, *Chem. Rev.,* **110**, 4724 (2010).
32. Z.-L. Wang, R. Guo, G.-R. Li, H.-L. Lu, Z.-Q. Liu, F.-M. Xiao, M. Zhang, and Y.-X. Tong, *J. Mater. Chem.,* **22**, 2401 (2012).
33. Z. Fan, J. Yan, T. Wei, L. Zhi, G. Ning, T. Li, and F. Wei, *Adv. Fun. Mater.,* **21**, 2366 (2011).
34. S. C. Sekhar, G. Nagaraju, and J. S. Yu, *Nano Energy,* **36**, 58 (2017).
35. X. Li, R. Liu, C. Xu, Y. Bai, X. Zhou, Y. Wang, and G. Yuan, *Adv. Fun. Mater.,* **28**, 1800064 (2018).
36. D. Wu and W. Zhong, *J. Mater. Chem. A,* **7**, 5819 (2019).
37. Y. Zou, R. Liu, W. Zhong, and W. Yang, *J. Mater. Chem. A,* **6**, 8568 (2018).
38. S. Peng, L. Fan, C. Wei, X. Liu, H. Zhang, W. Xu, and J. Xu, *Carbohydr. Polym.,* **157**, 344 (2017).